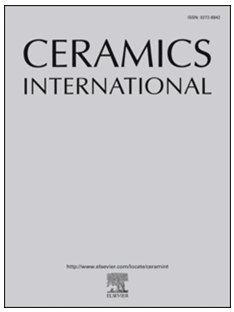

Thermoluminescence characteristics of monoclinic $SrAl_2O_4$ phosphor prepared by combustion method

N.R. Thejavathi, H.S. Lokesha, K.R. Nagabhushana, Sonia Hatsue Tatumi, S. Krishnaveni

PII: S0272-8842(24)00260-8

DOI: https://doi.org/10.1016/j.ceramint.2024.01.245

Reference: CERI 39568

To appear in: *Ceramics International*

Received Date: 26 October 2023

Revised Date: 4 January 2024

Accepted Date: 17 January 2024

Please cite this article as: N.R. Thejavathi, H.S. Lokesha, K.R. Nagabhushana, S.H. Tatumi, S. Krishnaveni, Thermoluminescence characteristics of monoclinic $SrAl_2O_4$ phosphor prepared by combustion method, *Ceramics International* (2024), doi: https://doi.org/10.1016/j.ceramint.2024.01.245.

Thermoluminescence characteristics of monoclinic $SrAl_2O_4$ phosphor prepared by combustion method

N.R. Thejavathi[1,2], H.S. Lokesha[3,4], K.R. Nagabhushana[3,4#], Sonia Hatsue Tatumi[3], Krishnaveni S[1*]

[1]Department of Studies in Physics, University of Mysore, Mysuru– 570 006, Karnataka, India

[2]Department of Physics, Government College (Autonomous), Mandya – 571 401, Karnataka, India

[3]Federal University of São Paulo, Campus Baixada Santista, CEP: 11070-100, Santos/SP – Brazil

[4]Department of Physics, Amity School of Applied Sciences, Amity University, Bengaluru – 562 110, Karnataka, India

[*]Corresponding Author: email: sk@physics.uni-mysore.ac.in; Phone: +91-98440 23568

[#]Corresponding Author: email: bhushankr@gmail.com, nagabhushanakr@blr.amity.edu

Abstract:

Thermoluminescence and its kinetic analysis, and defects in $SrAl_2O_4$ have been investigated. $SrAl_2O_4$ was synthesized by the solution combustion method. Rietveld refined X-ray diffraction pattern of $SrAl_2O_4$ reveals a monoclinic phase with space group $P2_1$. The average crystallite size and stain are 48 nm and 0.04%, respectively. The chemical composition of the sample is examined by the X-ray fluorescence technique. The micrographs of $SrAl_2O_4$ revealed that the particles are agglomerated with a porous nature. Defect centers involved in TL process is identified by EPR studies. TL of beta irradiated (40 Gy) $SrAl_2O_4$ displays three peaks and these peaks are reproducible at 104.4 ± 1.6 ^oC, 133.5 ± 1.0 ^oC and 260.5 ± 1.5 ^oC. In view of the TL curve being complex, the peaks analyzed using thermal cleaning and T_m-T_{stop} methods revealed that there are four peaks associated with the glow curve. The kinetic parameters are calculated using different techniques. TL peaks observed at 134 and 260 ^oC follow first order kinetics that is confirmed from qualitative and quantitative results. TL peak at 104 ^oC completely fades within 108000 s (30 h) whereas the intensity of 134 ^oC and 206 ^oC peak drops down to 63% and 2% of its initial value within 108000 s of irradiation. TL main peaks 1 and 2 are subject to thermal quenching, the activation is found to be 0.54±0.09 and 0.77±0.03 eV, respectively. This work elucidates the dosimetric features, kinetic analysis, and defects in undoped $SrAl_2O_4$.

Key Words: $SrAl_2O_4$, Combustion synthesis, Thermoluminescence, Kinetic parameters, Electron paramagnetic resonance.

1. Introduction:

Luminescent properties of aluminate-based materials (MAl_2O_4, M=Mg, Zn, Ca, Sr, Ba) are being studied due to their intense and unusual luminescent response [1–4]. Among the several aluminates, the strontium aluminate ($SrAl_2O_4$) has received attention due to excellent chemical stability and sensitive luminescence response behavior especially when this material is doped with rare earth (RE) elements with thermal treatments and irradiation with ionizing radiation [5,6]. The rare earth doped $SrAl_2O_4$ samples exhibit one of the longest afterglows among the broad range of inorganic persistent phosphors [7].

Thermoluminescence (TL) is an ideal technique to investigate the characteristics of traps and their distributions [8,9]. Glow curve shape and intensity depend on many factors including host material and its structure, dopants and their concentration, synthesis method and so on [10]. TL and afterglow properties of rare earth (Eu, Dy, Nd) doped $SrAl_2O_4$ have been widely studied [2,11–14]. However, dosimetric properties of undoped $SrAl_2O_4$ have not been explored thoroughly. Recently, Vitola et al. [15] reported TL of sol-gel synthesized $SrAl_2O_4$, the sample shows a peak at 147 ^oC under X-ray irradiation. Sonia et al. [16] reported that $SrAl_2O_4$ is in the monoclinic+cubic phase, TL curve shows a peak at 147 ^oC under X-ray irradiation. Combustion synthesized $SrAl_2O_4$ exhibits a broad TL peak at 48 ^oC under ultraviolet irradiation [17]. TL and EPR characteristics of solid state synthesized $SrAl_2O_4$ were reported by Edwar et al. [6]. Gamma rays irradiated $SrAl_2O_4$ show three TL peaks at 135, 260 and 350 ^oC and two defect centers (O^- ion and F^+ center) were identified from EPR results. The $SrAl_2O_4$ phosphor showed a good TL response under beta and gamma radiation as compared to other aluminates ($ZnAl_2O_4$ and $MgAl_2O_4$). However, a systematic study of the dosimetric features, kinetic analysis of the TL curve and thermal quenching information are lacking in the literature.

In the present work, $SrAl_2O_4$ phosphor was prepared by the combustion method. The phase purity of the sample is analyzed by Rietveld refinement of XRD data. The morphology and chemical composition of the sample are investigated using Scanning electron microscopy and X-ray fluorescence, respectively. The defects in $SrAl_2O_4$ are studied using electron paramagnetic resonance. TL dosimetric properties of $SrAl_2O_4$ are tested under beta irradiation. Kinetic analysis of the peaks is carried out using various methods. This work aims to contribute better understanding of the dosimetric features, kinetic analysis of TL peaks and defects in undoped $SrAl_2O_4$.

2. Experimental

Material Synthesis: Strontium aluminate ($SrAl_2O_4$) phosphor was synthesized by the solution combustion method. Strontium nitrate (≥ 99%), aluminum nitrate nanohydrate (≥ 98%) and glycine (≥ 98.5%) chemicals were purchased from Merck Company, India. These chemicals were used as initial reagents without further purification. The stoichiometry of the redox reactions was calculated using fundamental propellant chemistry ideas i.e., the ratio of the total oxidizing valence of metal nitrates and total reducing valence of fuels should be equal to unity. Stoichiometric amounts of nitrates were dissolved in 30 ml of double distilled water. The mixture was stirred until to get transparent solution then placed in a muffle furnace preheated to 400 ^{o}C. Initially, the solution boiled and dehydrated followed by combustion has taken place. Finally, the powder product was obtained and then ground into even more fine particles using an agate mortar and pestle. The sample was thereafter annealed at 1200 °C for two hours in a muffle furnace in an ambient atmosphere.

Characterization: Powder X-ray diffraction (PXRD) measurement was carried out using a Rigaku miniFlex 300 diffractometer. The micrograph of $SrAl_2O_4$ was measured using Quanta FEG 650 scanning electron microscope attached with an energy dispersive spectroscopy (EDS) Quantax microanalysis system. Elemental analysis of the sample was examined using Malvern Panalytical X-ray fluorescence spectrometer (Model: Zetium). The unirradiated $SrAl_2O_4$ monoclinic samples didn't show any TL or EPR response and hence the defects were created in the sample using beta and gamma ionizing radiation. The undoped $SrAl_2O_4$ samples were irradiated with the $^{90}Sr/^{90}Y$ beta radiation of energy 0.546 MeV with a dose rate of about 0.069 Gy s^{-1} and ^{60}Co gamma radiation of average energy 1.25 MeV. For TL measurements, the samples were irradiated in various doses between 5 and 100 Gy and for EPR measurements the sample was irradiated with 1 kGy gamma rays with a dose rate of 0.177 Gy s^{-1}. TL glow curves were recorded under BG 39 filter at a linear heating rate of 5 °C s^{-1} using a Risø TL/OSL reader (DA20). And a mask (a black paper with a 3 mm diameter hole) was used below the photomultiplier tube to avoid the intensity saturation during TL measurement. For EPR experiments, the required quantity of sample is 30 mg and the EPR signal is not detected for a lower dose (< 500 Gy) of gamma radiation. The experimental issue to perform EPR for beta radiation is the irradiation of the sample under beta radiation. In Risø TL/OSL reader, beta irradiation is possible at only < 10 mg on aliquot each time and it takes a long time for beta irradiation because of the low dose rate. Electron paramagnetic resonance (EPR) spectra were

measured using a Freiberg Instruments MiniScope ESR spectrometer Model 5500 at room temperature and operating at the X-band frequency. Instrument parameters: sweep time: 120 s, modulation amplitude: 0.1 mT, modulation frequency: 100 kHz, microwave power: 20 mW.

3. Results and discussions

3.1 X-ray diffraction

Rietveld refined XRD pattern of $SrAl_2O_4$ is shown in Figure 1. The undoped $SrAl_2O_4$ sample mainly exhibits two crystallographic phases, i.e. monoclinic with space group $P2_1$ and hexagonal with space group $P6_322$ [18]. However, in the present investigation, the diffraction peaks match well with the standard data (PDF # 2002284) which belongs to the monoclinic phase of $SrAl_2O_4$ with space group $P2_1$. Also, a small intense diffraction peak observed at $2\theta = 25.08°$ is not related to the monoclinic and hexagonal phases of $SrAl_2O_4$. According to the literature, the synthesized and commercial $SrAl_2O_4$ based materials show a small diffraction peak at $2\theta = 25°$ [19,20] and this peak coexists with the monoclinic structure of $SrAl_2O_4$ and that is related to $Sr_4Al_{14}O_{25}$ [18]. The lattice parameters and cell volume are obtained from Rietveld refinement analysis of the XRD pattern using the Crystallography Data Analysis Software GSAS II™ [21]. The values of lattice parameters (a = 8.4427 (2), b = 8.8267 (3), c = 5.1539 (1) Å) and cell volume = 383.42 Å^3 match well with standard data of monoclinic structure of the $SrAl_2O_4$ (a = 8.447, b = 8.816 and c = 5.163 Å, and 383.79 Å^3) respectively. The value of goodness of fit is 1.41, indicating a good match between theoretical and experimental data. The fitting parameters R_{wp} (%) and R_F (%) are 12.15% and 2.49%, respectively.

The crystallite size and strain were calculated using refinement parameters such as 2θ of the diffraction peak, full width at half maximum (FWHM) and interplanar spacing. The equation of the size-strain plot (SSP) method [22] is expressed as

$$\left(\frac{d_{hkl}\beta_{hkl}\,cos\theta}{\lambda}\right)^2 = \frac{k\lambda}{D}\left(\frac{d_{hkl}^2\beta_{hkl}\,cos\theta}{\lambda^2}\right) + \left(\frac{\varepsilon}{2\lambda}\right)^2 \qquad (1)$$

where λ is the wavelength of the X-ray, D is the crystallite size, ε is the strain and k is the shape factor (0.9). Plots of $\left(\frac{d_{hkl}\beta_{hkl}cos\theta}{\lambda}\right)^2$ as function of $\left(\frac{d_{hkl}^2\beta_{hkl}cos\theta}{\lambda^2}\right)$ exhibits linearly proportional that is shown in Figure 2. The crystallite size (D) and strain (ε) were determined from the slope and intercept of the linear fit to data, respectively. The average crystallite size and strain were found to be 48 nm and 0.04% respectively.

3.2 X-ray fluorescence

XRF spectroscopy is very sensitive to detecting traces of elements present in the synthesized product. To determine the chemical composition of the synthesized samples and their percentage, X-ray fluorescence spectroscopy was used. The chemical composition of $SrAl_2O_4$ sample annealed at 1200 °C was examined using X-ray fluorescence and the obtained XRF results are summarized in Table 1. The oxide composition of the sample is mainly composed of SrO (40%) and Al_2O_3 (58.2%) along with a small amount of SO_3, Na_2O, SiO_2, Cl, CaO, TiO_2, Fe_2O_3, ZnO and As_2O_3.

3.3 Scanning electron microscopy

The surface morphology and chemical composition of the $SrAl_2O_4$ were carried out using Scanning Electron Microscopy (SEM) and Energy Dispersive X-ray Spectroscopy (EDS), respectively. The SEM micrograph of the $SrAl_2O_4$ sample is illustrated in Figure 3(a). It is observed that the particles are agglomerated with a porous nature. Some of the particles appeared to be spherical along with different sizes. The foamy nature of the sample was obtained and this was caused by the release of large amounts of gases during the combustion process. Here, the smaller grains agglomerated and formed bigger particles when the sample was annealed at 1200 ^oC. EDS results revealed that there are three elements present in the sample such as Sr, Al, and O, and no other impurities detected in the measured limit (see Figure 3(b)).

3.4 Electron paramagnetic resonance

The EPR spectrum of pristine and gamma irradiated $SrAl_2O_4$ phosphor is shown in Figure 4. The EPR spectrum of gamma irradiated $SrAl_2O_4$ shows two distinct defect centers, these are labeled as Center I and Center II. The g-value of center I is 2.017 and it displays four hyperfine splitting. The linewidth of the individual hyperfine lines is about 12 G. The similar features as the center I was reported in solid-state synthesized $SrAl_2O_4$ [23] and $MgAl_2O_4$ [24]. Therefore, this Center I is assigned to O^- ion, it formed due to hole trapping at oxygen ions surrounding cation (possibly Sr or Al) vacancies. Moreover, the four hyperfines are not related to ^{27}Al and ^{87}Sr isotopes [23,25]. These hyperfine observed an interaction with an unknown impurity ion with nuclear spin 3/2. The linewidth center II is 5 gauss and a g-value equal to 2.0023 due to the F^+ center (singly ionized oxygen vacancy) [23].

3.5 Thermoluminescence

The thermoluminescence glow curve of $SrAl_2O_4$ phosphor measured for different doses from 5 to 100 Gy is shown in Figure 5. The glow curve shows a broad prominent peak between 50 and 220 ^oC and a secondary peak at 260 ^oC for the TL curve measured for a dose 40 Gy. In the broad peak, there are two discernible peaks observed at 104 and 134 ^oC. The reproducibility of peaks at 104 ^oC (labeled as peak 1), 134 ^oC (labeled as peak 2) and 260 ^oC (labeled as peak 3) were studied in TL measurements made consecutively on the same aliquot, the sample irradiated to 40 Gy each time. The positions of peaks 1, 2 and 3 were found to be reproducible at 104.4 ± 1.6 ^oC, 133.5 ± 1.0 ^oC and 260.5 ± 1.5 ^oC respectively in a set of ten repetitive TL measurements. Zhai et al. [17] reported TL of $SrAl_2O_4$ prepared by combustion method with glycine as fuel, TL curve under UV irradiation (254 nm) shows a broad peak with peak maxima at 48 ^oC at a heating rate 2 °C s^{-1}. Solid state synthesized gamma irradiated $SrAl_2O_4$ exhibit TL peaks at 135, 260 and 350 ^oC, which was measured at a heating rate 5 °C s^{-1} [6]. Further, TL glow curves of $SrAl_2O_4$ were recorded for 100 Gy of beta and gamma radiation after 30 hours and shown in Figure 6. TL curves show two prominent peaks, the first peak appeared at 150 ^oC and 152 ^oC for beta and gamma irradiated samples and the second peak at 260 ^oC for both beta and gamma irradiated samples. However, there is a difference in intensity due to the difference in dose rate and energy of the beta and gamma radiation.

TL peak intensity as a function of beta dose from 5 to 100 Gy is shown in Figure 7 (a). It is observed that all the peaks intensity increases with an increase in dose. TL peaks intensity behavior with doses is analyzed using the superlinearity index f(D), the relation expressed as

$$f(D) = \left[\frac{y(D)/D}{y(D_1)/D_1}\right] \qquad (2)$$

where y(D) is the TL intensity at a dose D and $y(D_1)$ is the TL intensity at a low dose D_1. A value of f(D) = 1 represents a linear dose response, f(D) > 1 denotes supralinearity and f(D) < 1 indicates sublinearity. In the present work, the dose response of peaks 1 and 2 exhibits linear (f(D) = ~1) between 10 to 60 Gy and then peaks intensity increases supralinearly with a dose up to 100 Gy. And peak 3 shows linear up to 20 Gy and supralinear between 20 to 100 Gy. Solid state synthesized $SrAl_2O_4$ also shows that the 260 ^oC peak increases sublinearly with dose thereafter 10 Gy [6].

The dependence of peak position on dose was used to assess the order of kinetics. The peak maxima (T_m) of peaks 1, 2 and 3 against doses between 5 - 100 Gy are shown in Figure 7(b). The position of peaks 1 and 3 changes from 94 to 114 ^oC and 272 to 250 ^oC, respectively when the dose increases from 5 to 100 Gy. However, peak 3 is stable at 260 ^oC within the dose between 40 to 70 Gy. In the case of peak 2, the T_m is stable at 132 ^oC and 134 ^oC for doses within 10–35 Gy and 40–100 Gy, respectively. It clearly shows that peak maxima changes for specific irradiation doses representing that peak 2 consists of multiple first-order peaks that individually become prominent at specific irradiation doses [14,26]. Results of T_m as a function dose signify that peak 2 follows first order kinetics.

To confirm the presence of any peaks collocated with the main peak on its higher temperature end, the thermal cleaning technique was used [27,28]. In the experiment, a sample was irradiated to 40 Gy and heated to 126 ^oC that is beyond the first peak maximum and cooled to 20 ^oC. Then the sample was heated again from ambient temperature to 400 ^oC. It is noted that after partial heating to 166 ^oC, the TL curve shows a different peak at 184 ^oC (labeled as Peak 2a) that is beyond peak 2 (134 ^oC). The experiments were repeated for different preheating to 234 and 330 ^oC, and as shown in Figure 8. Therefore, the result of thermal cleaning suggests that there are four peaks associated with the TL curve between 30 to 350 ^oC. The maxima of four peaks are observed at 102, 134, 184 and 262 ^oC.

To study the order of kinetics of the peaks, the T_m-T_{stop} method [10] was used. In the measurement, the sample was irradiated to 40 Gy and partially heated to 30 °C at a constant heating rate of 5 °C s^{-1} and cooled to 20 °C. The sample was reheated to measure the complete glow-curve and peak temperature position, T_m of main peaks was noted. The sample was freshly irradiated to 40 Gy and the procedure was repeated several times, each time T_{stop} increased in steps of 5 °C from 30 to 300 °C. Figure 9 shows the plot of peak temperature T_m against T_{stop}. According to TL theory [28], T_m displays a flat region against T_{stop} corresponding to a TL peak. The T_m-T_{stop} analysis revealed there are at least four peaks associated with the glow curve. This result matches well with the result of thermal cleaning. It is observed that T_m of peak 2 and peak 3 are independent of T_{stop} in two neighbouring regions at 134 and 140 °C, and 260 and 264°C, respectively. This behaviour indicates that the apparently single peak 2 and 3 consists of multiple first order components [29]. In case of peak 1 and peak 2a, the T_m increases with increase of T_{stop} suggests that the apparently single peak is a composite [5].

3.6 Evaluation of kinetic parameters

In the present work, kinetic parameters of the traps such as activation energy (*E*), frequency factor (*s*) and order of kinetics (*b*) of each peak are calculated using the whole glow peak (WGP), Chen's peak shape (CPS), glow curve deconvolution (GCD) and variable heating rate (VHR) methods. Among these methods, the glow curve deconvolution (GCD) method is developed using a general order kinetic equation [30] and it is useful to estimate the trap parameters of multiple-isolated peaks present in the TL curve. The details of the methods have been discussed elsewhere [28,29].

3.6.1 Whole glow peak method

In the WGP method, area (n) under the glow peak is linked with the order of kinetics (b), and the equation [28] can be expressed as,

$$ln\left(\frac{TL_{exp}}{n^b}\right) = ln\left(\frac{S'}{\beta}\right) - \left(\frac{E}{kT}\right) \quad (3)$$

Here, β is the heating rate and k is Boltzmann's constant (8.617×10^{-5} eV K^{-1}) and s' is the effective frequency factor for general order kinetics. The plot of $ln\left(\frac{TL_{exp}}{n^b}\right)$ versus $\frac{1}{kT}$ shows linear for a particular value of the order of kinetic (*b*) and as shown in Figure 10. The peaks 1, 2, 2a and 3 are best fitted (R^2 = 0.997) for the value of b is 1.5, 1.5, 2 and 1.25, respectively. The values of *E* and *s* are obtained from the slope and y-axis intercept of the straight line respectively. The calculated kinetic parameters are given in Table 2.

3.6.2 Peak shape method

The activation energy of the peaks was calculated using the peak shape method [28]. The peak shape relation is

$$E_\alpha = C_\alpha\left(\frac{k\,T_m{}^2}{\alpha}\right) - b_\alpha(2kT_m) \quad (4)$$

where α stands for τ, δ and ω, T_m is the peak maxima, the c_α and b_α are constants. The TL peak 2 is shown in Figure 11. The τ is refers to the half-width on the rising side of the TL peak, δ is the half-width at the fall-off side (δ) of the TL peak and ω is the full width at half maximum. The geometrical factor, $\mu = \delta/\omega$ value varies from 0.36 to 0.55 for the order of kinetics values between 0.7 and 2.5, respectively [28]. The average activation energy of E_τ, E_δ and E_ω of the peaks are tabulated in Table 2. The calculated geometrical factors are 0.51, 0.50, 0.52 and 0.46 for peaks 1, 2, 2a and 3, respectively. These values indicate that peaks 1, 2 and 2a follow non-first order kinetics and peak 3 follows first order kinetics.

3.6.3 Glow curve deconvolution

Kinetic parameters of the glow peaks were analyzed by curve fitting using the glow curve deconvolution (GCD) method [31,32]. The general order kinetic equation of temperature dependence of the TL intensity is described as

$$I(T) = I_m b^{\frac{b}{b-1}} \left(\frac{E}{kT}\frac{T-T_m}{T_m}\right) \times [(b-1)(1-\Delta)\frac{T^2}{{T_m}^2}\exp\left(\frac{E}{kT}\frac{T-T_m}{T_m}\right) + Z_m]^{-\frac{b}{b-1}} \qquad (5)$$

Where, $\Delta = 2kT/E$, $\Delta_m = 2kT_m/E$, $Z_m = 1 + (b-1)\Delta_m$ and I_m is peak maximum intensity. The software package Microsoft Excel with the solver utility was used for curve fitting. The deconvoluted glow curve is shown in Figure 12. Here, the TL curve is best fitted to four peaks that good agreement with the number of peaks associated with the glow curve estimated from the thermal cleaning and T_m-T_{stop} methods. The figure of merit of fit is 1.76 and the residuals of GCD fluctuate about zero, indicating a good fit between the experimental and theoretical profile. The frequency factor conveys value in the order of the lattice vibration frequency. The frequency factor of each peak was calculated by using the general order equation,

$$s = \frac{\beta E}{{kT_m}^2}\frac{1}{Z_m}\exp\left(\frac{E}{kT_m}\right) \qquad (6)$$

The kinetic parameters calculated for all four peaks are tabulated in Table 2. The order of kinetic of the peaks 1, 2, 2a and 3 was found to be 1.9, 1.34, 2 and 1.8, respectively. Here, the peaks 1, 2a and 3 follow non-first order kinetics. This indicates that the occurrence of the traps which are due to the re-trapping phenomena [33]. The peak 2 follows first order kinetics.

3.6.4 Variable heating rate method

The variable heating rate was applied to calculate the kinetic parameters of the main peaks. The relation of heating rate, peak temperature maxima and activation energy is expressed as

$$ln\left(\frac{T_m^2}{\beta}\right) = ln\left(\frac{E}{sk}\right) + \left(\frac{E}{kT_m}\right) \qquad (7)$$

The plot of $ln\left(\frac{T_m^2}{\beta}\right)$ vs $\left(\frac{1}{kT_m}\right)$ exhibits a straight line, as shown in Figure 13. The slope of a straight line gives activation energy *E*, and the intercept of the line is equal to $ln\left(\frac{E}{sk}\right)$. The values of *E* of each peak are given in Table 2. The frequency of bound electrons is an attempt to detach from its binding potential that is in the order of 10^{10} to 10^{12} s^{-1}.

The TL intensity of peaks 1 and 2 decreases with the increase of heating rate from 1 to 7 °C s^{-1} as shown in Figure 14. This indicates that main peaks are affected by thermal

quenching. The activation energy for thermal quenching *W* can be calculated by using the temperature dependence of the luminescence efficiency expressed by,

$$\eta(T) = \frac{I_q}{I_{uq}} = \frac{1}{1+C\exp(-W/kT_m)} \quad (8)$$

here I_{uq} represents where the quenching is minimal, I_q represents the intensity of the glow curve where the quenching is high and *C* is a constant. The plot of $\ln[(I_{uq}/I_q)-1]$ versus $1/kT_m$ for peaks 1 and 2 is shown in Figure 15. The values of *W* and *C* were found from the slope and intercept of the fit data. The values of *W* and *C* are 0.54±0.09 and 0.77±0.03 eV, and 2.60×10^{10} and 6.59×10^{12} for peaks 1 and 2, respectively. To the best of our knowledge, this is the first time these values have been reported for undoped $SrAl_2O_4$.

3.6.5 Fading

To study fading, TL glow curves of $SrAl_2O_4$ were recorded at different intervals of time between irradiation and readout. Figure 16 shows the TL peak intensities of $SrAl_2O_4$ fade with the increase in storage time between irradiation and TL readout. Each peak intensities are normalized by dividing by their respective intensity measured immediately after irradiation. The intensity of peak 1 (peak at 104 °C) is completely faded within 108000 s. In the case of peak 2, the peak intensity decreased by 6% over 1800 s but the peak 2 intensity drops to 63% of its initial intensity after 108000 s. Meanwhile, peak 3 is stable at room temperature and the peak intensity reduced by only 2% is observed (108000 s). In addition, the position of all peaks is independent of storage time.

In the present work, the shape of TL curve and peaks position different than the $SrAl_2O_4$ prepared using sol-gel and and solid-state synthesized undoped $SrAl_2O_4$ [16,23]. Thermal cleaning and T_m-T_{stop} analysis confirmed there are four peaks associated with TL curve. The activation energy of the TL peaks assessed by whole glow peak, peak shape, glow curve deconvolution and variable heating rate methods are consistent. Edwar et al. [23] reported a higher value of activation energy estimated by curve fitting for peaks at 137 and 261 ^oC were 1.05 and 1.60 eV respectively. Furthermore, they concluded that these peaks follow non-first order kinetics. In the present work, the activation energy of 134 and 260 ^oC peaks were found to be 0.87 and 1.02 eV and these peaks follow first order kinetics confirmed from various methods. The type of defects generated during irradiation of ionizing radiation is dependent on radiation weighting factors. However, the concentration of defects created due to ionizing radiation depends on the energy and dose rate of the radiation. Here, the radiation weighting

factor of both gamma and beta radiations is the same and equal to 1 for all energies [34]. Hence, the type of defects generated in the sample under gamma and beta radiation are the same. The correlation of fading, EPR and TL result suggests that peak 1 is related to F^+ center and the O^- ion center is associated with the TL peaks 2 and 3. The quenching activation energy for peaks 1 and 2 are 0.54±0.09 and 0.77±0.03 eV, respectively. This thermal quenching might be caused due to thermal ionization at the excited state of F^+ center [35].

4. Conclusion

A monoclinic phase of $SrAl_2O_4$ was prepared by the combustion method. The structural parameters were assessed using the Rietveld refinement of the XRD pattern. X-ray fluorescence results revealed the elements present in synthesized $SrAl_2O_4$. The thermal cleaning and T_m-T_{stop} methods revealed that there are four peaks associated with the glow curve, peaks maxima at 104, 134, 184 and 262 ºC. The kinetic parameters of all four peaks were calculated using various methods. The dose response and fading of the peaks were studied. TL and EPR correlation reveal O^- ion and F^+ centers are responsible for TL traps. Both peak 1 and 2 are affected by thermal quenching, the corresponding activation energy was found to be 0.54±0.09 and 0.77±0.03 eV, respectively. This work shows TL properties and defects in undoped $SrAl_2O_4$.

Acknowledgements

The authors dedicate this paper to Prof. Dr. B.N. Lakshminarasappa, a retired professor of Physics, Bangalore University, Bengaluru, Karnataka, India who passed away on January 02, 2024. He was a real fine experimentalist and a source of inspiration for many researchers.

References:

[1] V. Singh, S. Watanabe, T.K. Gundu Rao, J.F.D. Chubaci, I. Ledoux-Rak, H.Y. Kwak, Infrared luminescence, thermoluminescence and defect centres in Er and Yb co-doped $ZnAl_2O_4$ phosphor, Appl. Phys. B Lasers Opt. 98 (2010) 165–172. https://doi.org/10.1007/s00340-009-3766-7.

[2] V. Chernov, P. Salas-Castillo, L.A. Díaz-Torres, N.J. Zúñiga-Rivera, R. Ruiz-Torres, R. Meléndrez, M. Barboza-Flores, Thermoluminescence and infrared stimulated luminescence in long persistent monoclinic $SrAl_2O_4:Eu^{2+},Dy^{3+}$ and $SrAl_2O_4:Eu^{2+},Nd^{3+}$ phosphors, Opt. Mater. (Amst.) 92 (2019) 46–52. https://doi.org/10.1016/j.optmat.2019.04.015.

[3] R.K. Gartia, M.N. Singh, L.P. Chanu, T.B. Singh, Determination of thermoluminescence parameters in nanocrystalline $CaAl_2O_4$, J. Lumin. 219 (2020) 116867. https://doi.org/10.1016/j.jlumin.2019.116867.

[4] S.S. Raj, D.R. Mishra, A. Soni, V. Grover, G.S. Polymeris, K.P. Muthe, S.K. Jha, A.K. Tyagi, TL and OSL studies of carbon doped magnesium aluminate (MgAl2O4: C), Radiat. Phys. Chem. 127 (2016) 78–84. https://doi.org/10.1016/j.radphyschem.2016.06.007.

[5] M.L. Chithambo, A.H. Wako, A.A. Finch, Thermoluminescence of $SrAl_2O_4:Eu^{2+}$, Dy^{3+}: Kinetic analysis of a composite-peak, Radiat. Meas. 97 (2017) 1–13. https://doi.org/10.1016/j.radmeas.2016.12.009.

[6] E.A. Canaza-Mamani, N.F. Cano, J. Mosqueira-Yauri, T.K.G. Rao, S.C. Aynaya-Cahui, A.J. Gonsalez-Vasquez, M.B. Gomes, J.F.D. Chubaci, S. Watanabe, J.S. Ayala-Arenas, TL and EPR characteristics of $SrAl_2O_4$ phosphor prepared by solid-state reaction method, J. Lumin. 245 (2022). https://doi.org/10.1016/j.jlumin.2021.118585.

[7] R.E. Rojas-Hernandez, F. Rubio-Marcos, M.Á. Rodriguez, J.F. Fernandez, Long lasting phosphors: $SrAl_2O_4$:Eu, Dy as the most studied material, Renew. Sustain. Energy Rev. 81 (2018) 2759–2770. https://doi.org/10.1016/j.rser.2017.06.081.

[8] R. Chen, S.W.S. McKeever, Theory of Thermoluminescence and Related Phenomena, Theory of Thermoluminescence and Related Phenomena, World Scientific, 1997. https://doi.org/10.1142/2781.

[9] A.J.J. Bos, Thermoluminescence as a research tool to investigate luminescence mechanisms, Materials 10 (2017). https://doi.org/10.3390/ma10121357.

[10] S.W.S. McKeever, Thermoluminescence of solids, Cambridge University Press, 1985.

[11] H. Hagemann, D. Lovy, S. Yoon, S. Pokrant, N. Gartmann, B. Walfort, J. Bierwagen, Wavelength dependent loading of traps in the persistent phosphor $SrAl_2O_4:Eu^{2+}$, Dy^{3+}, J. Lumin. 170 (2016) 299–304. https://doi.org/10.1016/j.jlumin.2015.10.035.

[12] T. Delgado, J. Afshani, H. Hagemann, Spectroscopic study of a single crystal of $SrAl_2O_4:Eu^{2+}:Dy^{3+}$, J. Phys. Chem. C. 123 (2019) 8607–8613. https://doi.org/10.1021/acs.jpcc.8b12568.

[13] D. Van der Heggen, D. Vandenberghe, N.K. Moayed, J. De Grave, P.F. Smet, J.J. Joos, The almost hidden role of deep traps when measuring afterglow and thermoluminescence of persistent phosphors, J. Lumin. 226 (2020) 117496. https://doi.org/10.1016/j.jlumin.2020.117496.

[14] M.L. Chithambo, Thermoluminescence of the main peak in $SrAl_2O_4:Eu^{2+}$, Dy^{3+}: Spectral and kinetics features of secondary emission detected in the ultra-violet region, Radiat. Meas. 96 (2017) 29–41. https://doi.org/10.1016/j.radmeas.2016.12.001.

[15] V. Vitola, D. Millers, K. Smits, I. Bite, A. Zolotarjovs, The search for defects in undoped $SrAl_2O^4$ material, Opt. Mater. (Amst.) 87 (2019) 48–52. https://doi.org/10.1016/j.optmat.2018.06.004.

[16] S.H. Tatumi, A. de F. Soares, D.R.G. Tudela, K.A. Gonçalves, R.R. Rocca, Sol-gel synthesis of strontium aluminate phosphor and its TL and OSL properties, Radiat. Phys. Chem. 157 (2019) 15–21. https://doi.org/10.1016/j.radphyschem.2018.12.013.

[17] B.G. Zhai, Y.M. Huang, Green afterglow of undoped $SrAl_2O_4$, Nanomaterials 11 (2021) 2–19. https://doi.org/10.3390/nano11092331.

[18] R.E. Rojas-Hernandez, F. Rubio-Marcos, A. Serrano, A. Rakhmatullin, C. Bessada, J.F. Fernandez, Unveiling the role of the hexagonal polymorph on $SrAl_2O_4$-based phosphors, RSC. Adv. 8 (2018) 28918–28927. https://doi.org/10.1039/c8ra05601c.

[19] V. Loryuenyong, J. Kornsawat, W. Nakhowong, W. Klinjan, A. Buasri, V. Loryuenyong, The temperature-dependent structural and optical properties of $SrAl_2O_4$-based phosphor, IOP Conf. Ser. Mater. Sci. Eng., 2020. https://doi.org/10.1088/1757-899X/965/1/012028.

[20] V.P. Singh, S.B. Rai, H. Mishra, C. Rath, Stabilization of high temperature hexagonal phase of $SrAl_2O_4$ at room temperature: Role of ZnO, Dalton Trans. 43 (2014) 5309–5316. https://doi.org/10.1039/c3dt52869c.

[21] B.H. Toby, R.B. Von Dreele, GSAS-II: The genesis of a modern open-source all purpose crystallography software package, J. Appl. Crystallogr. 46 (2013) 544–549. https://doi.org/10.1107/S0021889813003531.

[22] S. Kumar, K. Asokan, R.K. Singh, S. Chatterjee, D. Kanjilal, A.K. Ghosh, Investigations on structural and optical properties of ZnO and ZnO:Co nanoparticles under dense electronic excitations, RSC. Adv. 4 (2014) 62123–62131. https://doi.org/10.1039/c4ra09937k.

[23] E.A. Canaza-Mamani, N.F. Cano, J. Mosqueira-Yauri, T.K.G. Rao, S.C. Aynaya-Cahui, A.J. Gonsalez-Vasquez, M.B. Gomes, J.F.D. Chubaci, S. Watanabe, J.S. Ayala-Arenas, TL and EPR characteristics of $SrAl_2O_4$ phosphor prepared by solid-state reaction method, J. Lumin. 245 (2022). https://doi.org/10.1016/j.jlumin.2021.118585.

[24] A. Ibarra, F. J. Lopez, M. Jimenez de Castro, V centers in $MgAl_2O_4$ spinels, Phys. Rev. B 44 (1991) 7256–7262.

[25] M.S. Holston, J.W. McClory, N.C. Giles, L.E. Halliburton, Radiation-induced defects in $LiAlO_2$ crystals: Holes trapped by lithium vacancies and their role in thermoluminescence, J. Lumin. 160 (2015) 43–49. https://doi.org/10.1016/j.jlumin.2014.11.018.

[26] S. Thomas, J.M. Kalita, M.L. Chithambo, O.M. Ntwaeaborwa, The influence of dopants on thermoluminescence of $Sr_2MgSi_2O_7$, J. Lumin. 208 (2019) 104–107. https://doi.org/10.1016/j.jlumin.2018.12.035.

[27] J.M. Kalita, M.L. Chithambo, Thermoluminescence of α-Al_2O_3:C,Mg: Kinetic analysis of the main glow peak, J. Lumin. 182 (2017) 177–182. https://doi.org/10.1016/j.jlumin.2016.10.031.

[28] V. Pagonis, G. Kitis, C. Furetta, Numerical and practical exercises in thermoluminescence, Springer, 2006. https://doi.org/10.1007/0-387-30090-2.

[29] H.S. Lokesha, M.L. Chithambo, A combined study of the thermoluminescence and electron paramagnetic resonance of point defects in ZrO_2:Er^{3+}, Radiat. Phys. Chem. 172 (2020) 108767. https://doi.org/10.1016/j.radphyschem.2020.108767.

[30] G. Kitis, J.M. Gomez-Ros, J.W. N Tuyn, Thermoluminescence glow-curve deconvolution functions for first, second and general orders of kinetics, J. Phy. D: Appl. Phys. 31 (1998) 2636-2641.

[31] D. Afouxenidis, G.S. Polymeris, N.C. Tsirliganis, G. Kitis, Computerised curve deconvolution of TL/OSL curves using a popular spreadsheet program, Radiat. Prot. Dosimetry 149 (2012) 363–370. https://doi.org/10.1093/rpd/ncr315.

[32] G. Kitis, J.M. Gomez-Ros, J.W.N. Tuyn, Thermoluminescence glow-curve deconvolution functions for first, second and general orders of kinetics, J. Phys. D. Appl. Phys. 31 (1998) 2636–2641. https://doi.org/10.1088/0022-3727/31/19/037.

[33] P. Gupta, A.K. Bedyal, V. Kumar, V.K. Singh, Y. Khajuria, O.M. Ntwaeaborwa, H.C. Swart, Thermoluminescence and glow curves analysis of γ-exposed Eu^{3+} doped $K_3Y(PO_4)_2$ nanophosphors, Mater Res Bull 73 (2016) 111–118. https://doi.org/10.1016/j.materresbull.2015.08.030.

[34] W. Muhammad, A. Hussain, M. Maqbool, Basic Concepts in Radiation Dosimetry, in: M. Maqbool (Eds.), An introduction to medical physics, Springer, 2017, pp. 9–41. https://doi.org/10.1007/978-3-319-61540-0_2.

[35] S. V. Nikiforov, V.S. Kortov, D.L. Savushkin, A.S. Vokhmintsev, I.A. Weinstein, Thermal quenching of luminescence in nanostructured monoclinic zirconium dioxide, Radiat. Meas. 106 (2017) 155–160. https://doi.org/10.1016/j.radmeas.2017.03.020.

Tables

Table 1. Chemical composition of $SrAl_2O_4$ obtained from XRF result.

Sample	Weight %
SrO	40.0
Al_2O_3	58.2
SO_3	0.58
Na_2O	0.25
SiO_2	0.18
Cl	0.31
CaO	0.10
TiO_2	0.06
Fe_2O_3	0.06
ZnO	0.31
As_2O_3	0.02

Table 2. Summary of kinetic parameters estimated from various analysis methods.

Method	peaks	E (eV)	s (s^{-1})
WGP	1	0.69	1.16×10^{8}
	2	0.88	7.41×10^{8}
	2a	0.95	5.16×10^{9}
	3	1.09	1.30×10^{10}
CPS	1	0.76	
	2	0.89	
	2a	0.96	
	3	1.11	
GCD	1	0.68	5.89×10^{8}
	2	0.87	1.54×10^{10}
	2a	0.93	8.15×10^{9}
	3	1.02	7.10×10^{8}
VHR	1	0.64	4.45×10^{10}
	2	0.99	6.82×10^{11}
	3	1.3	1.63×10^{12}

Figures

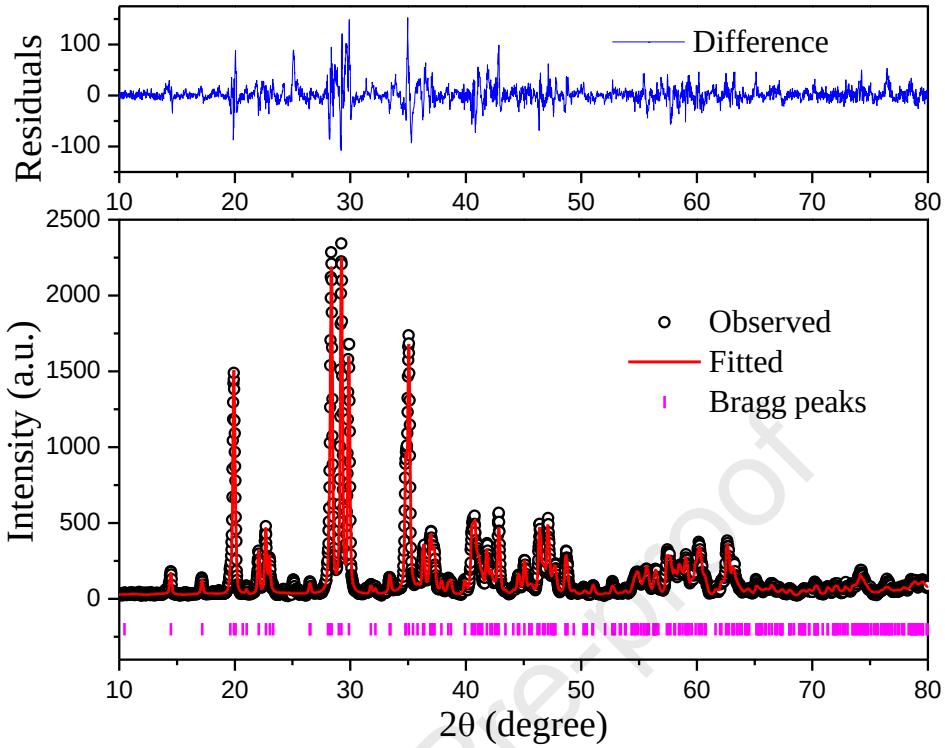

Figure 1. Rietveld refined XRD patterns of $SrAl_2O_4$. The black open symbols represent the experimental XRD data. This is compared with the calculated profile (red line). The small purple vertical lines below the curve are the expected Bragg positions of monoclinic structure $SrAl_2O_4$. The residual of the refinement is shown as a blue solid line.

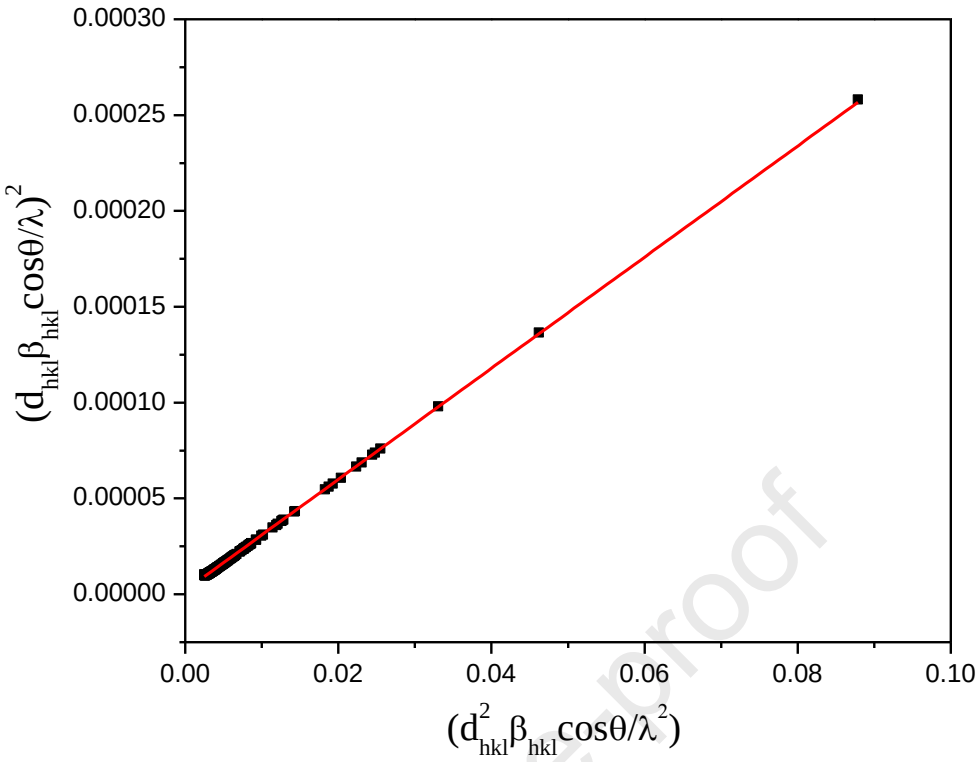

Figure 2. Plots of $\left(\frac{d_{hkl}\beta_{hkl}cos\theta}{\lambda}\right)^2$ as a function of $\left(\frac{d^2_{hkl}\beta_{hkl}cos\theta}{\lambda^2}\right)$ for $SrAl_2O_4$.

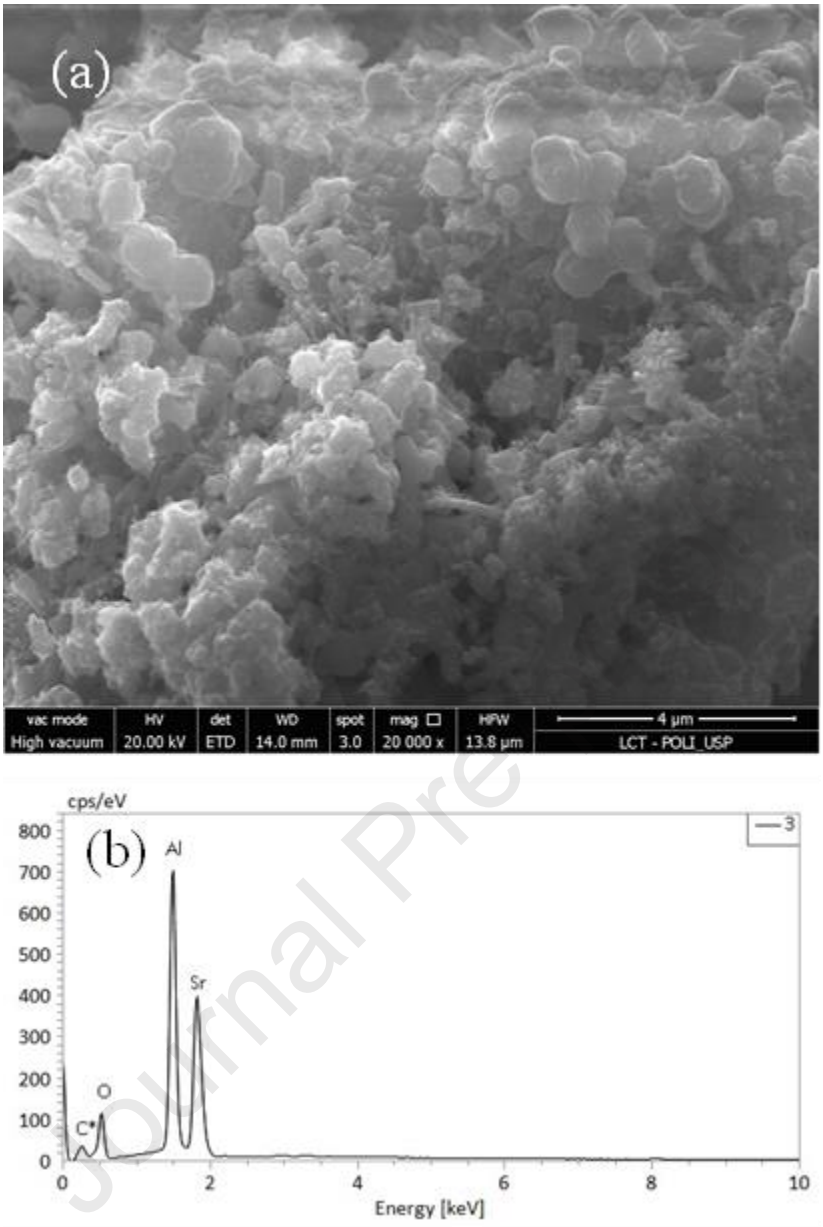

Figure 3. (a) SEM micrograph of $SrAl_2O_4$ and (b) EDX graph of $SrAl_2O_4$.

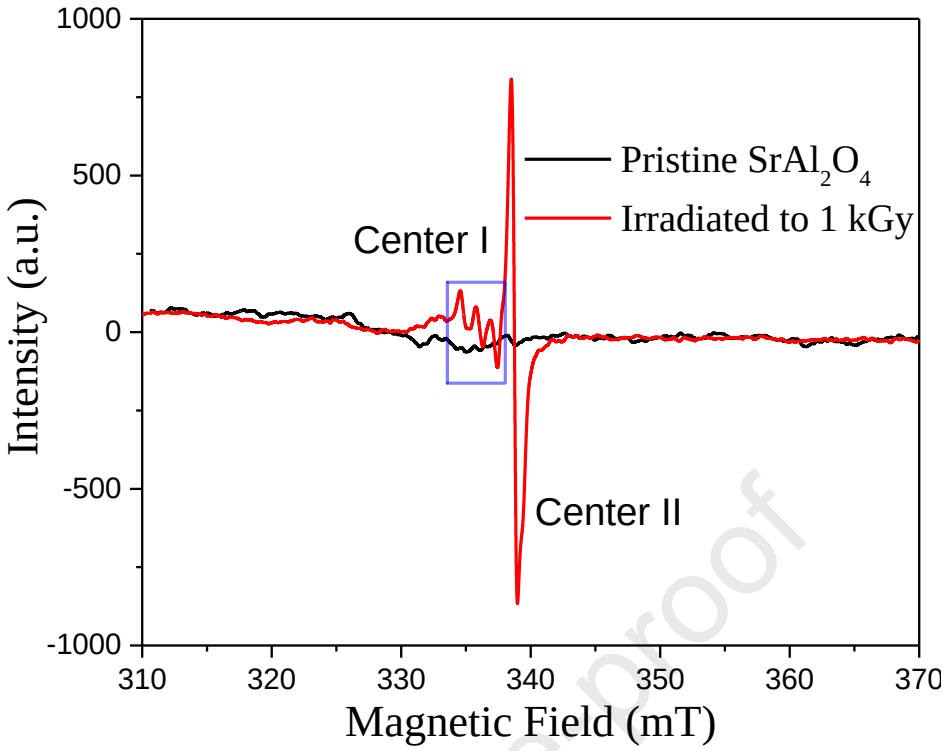

Figure 4. Room temperature EPR spectrum of pristine and gamma irradiated (1 kGy) $SrAl_2O_4$ phosphor.

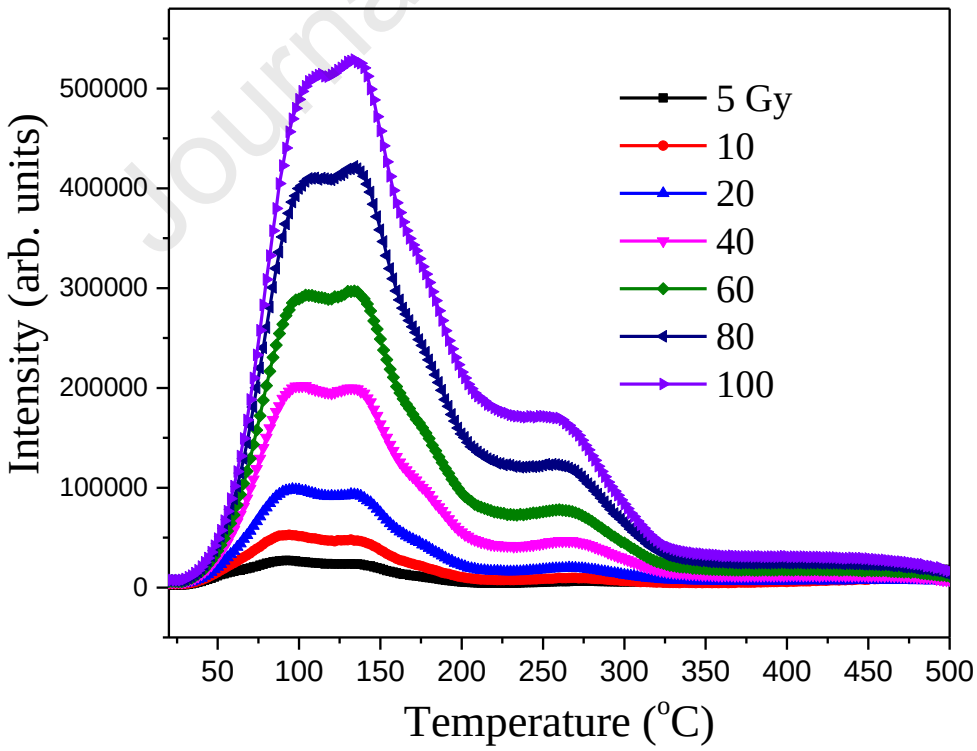

Figure 5. TL glow curves of $SrAl_2O_4$ measured for different doses.

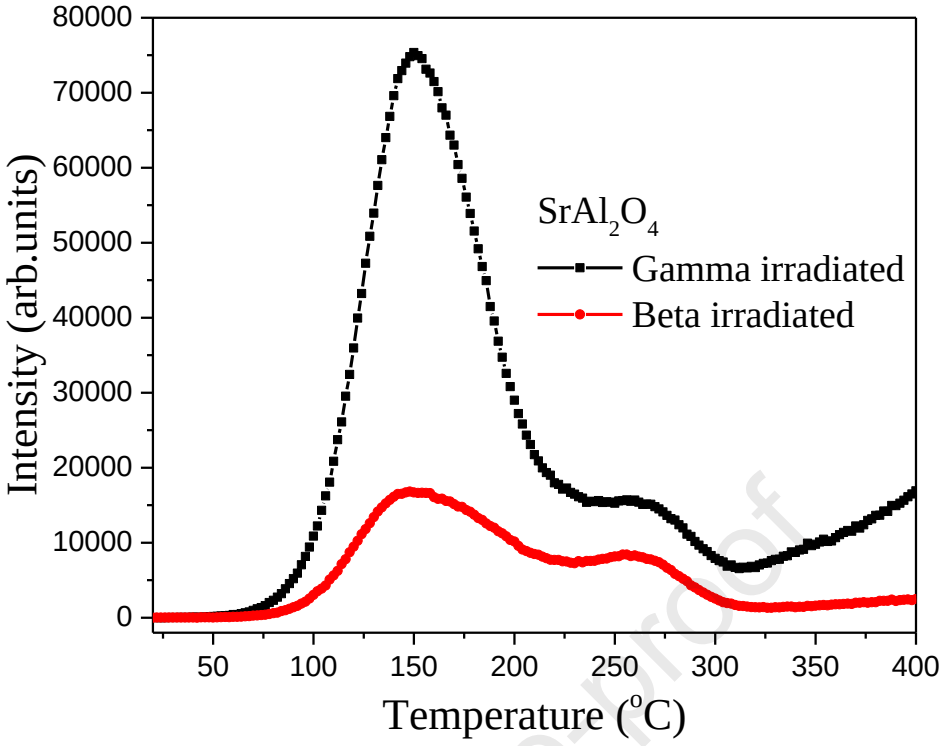

Figure 6. TL glow curves of beta and gamma irradiated $SrAl_2O_4$ for 100 Gy.

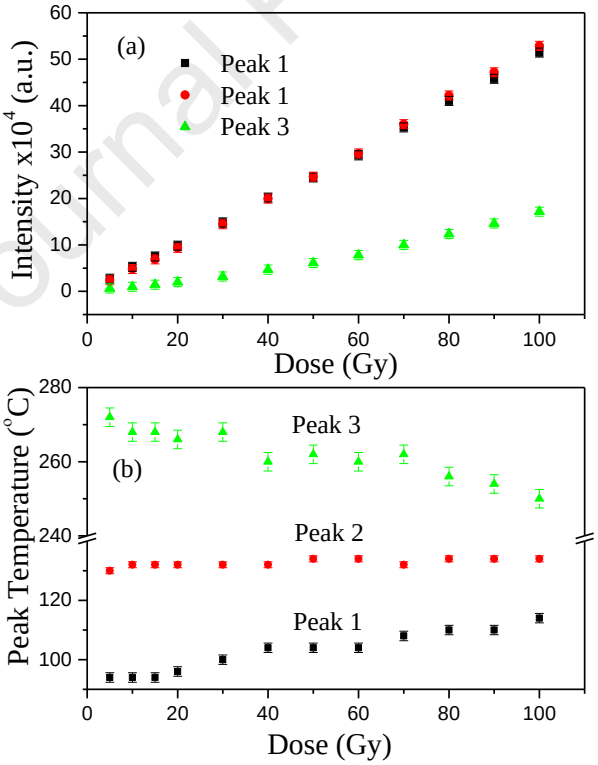

Figure 7. (a) Variation of TL intensity of the peaks as a function of doses and (b) Temperature maxima of the peaks as a function of doses.

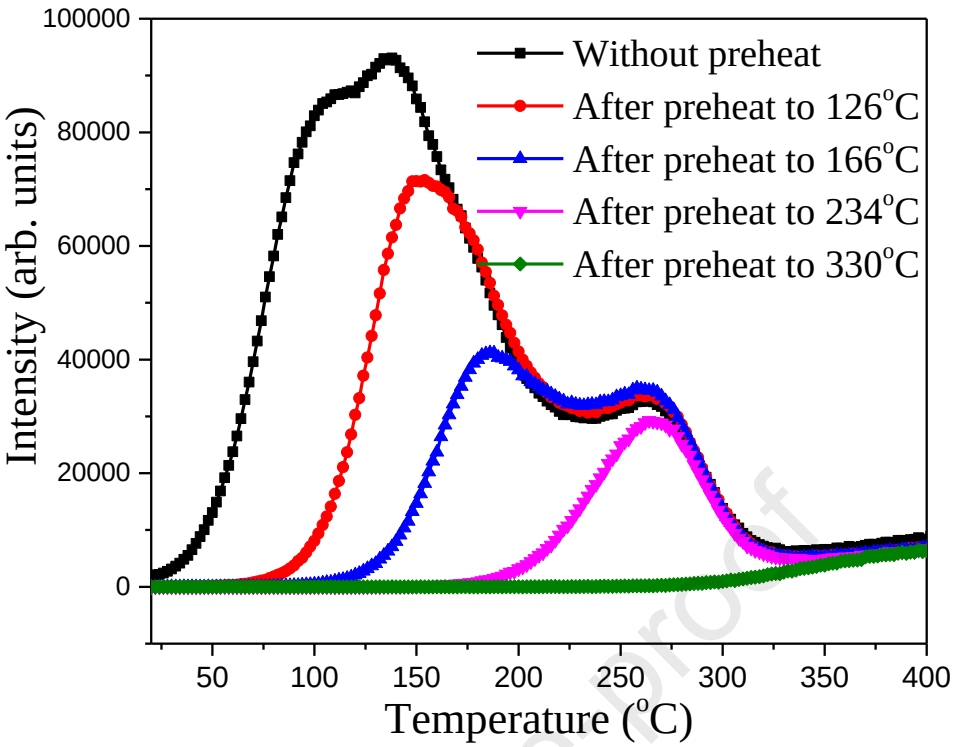

Figure 8. TL glow curve resolution of $SrAl_2O_4$ using thermal cleaning procedure, the sample irradiated to 40 Gy.

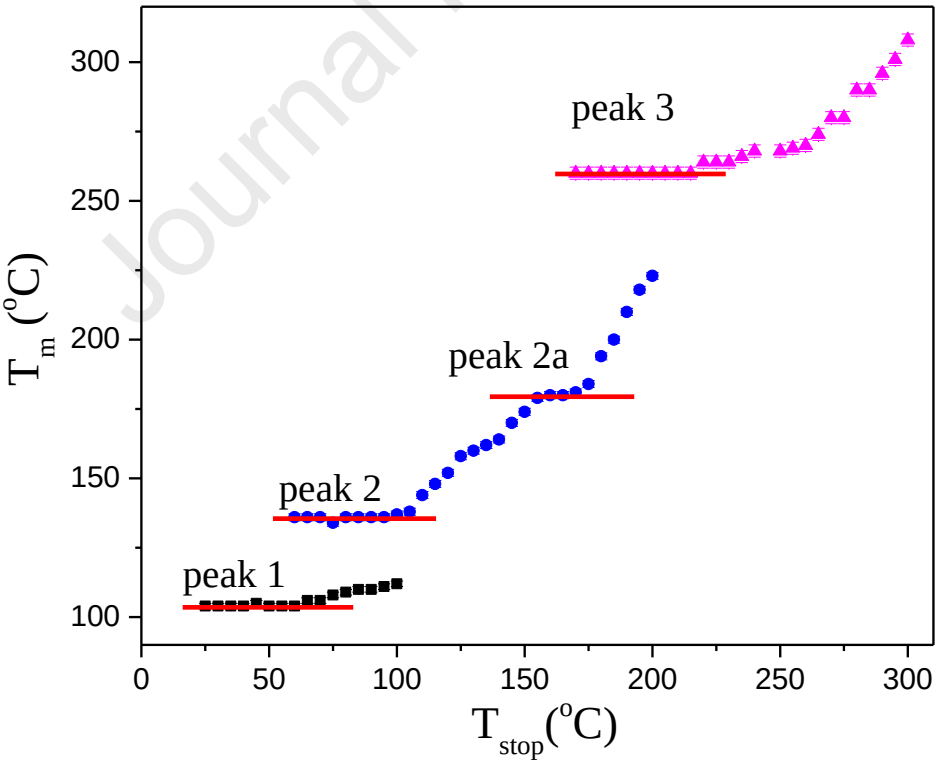

Figure 9. T_m-T_{stop} curve of $SrAl_2O_4$ phosphor irradiated to a dose of 40 Gy.

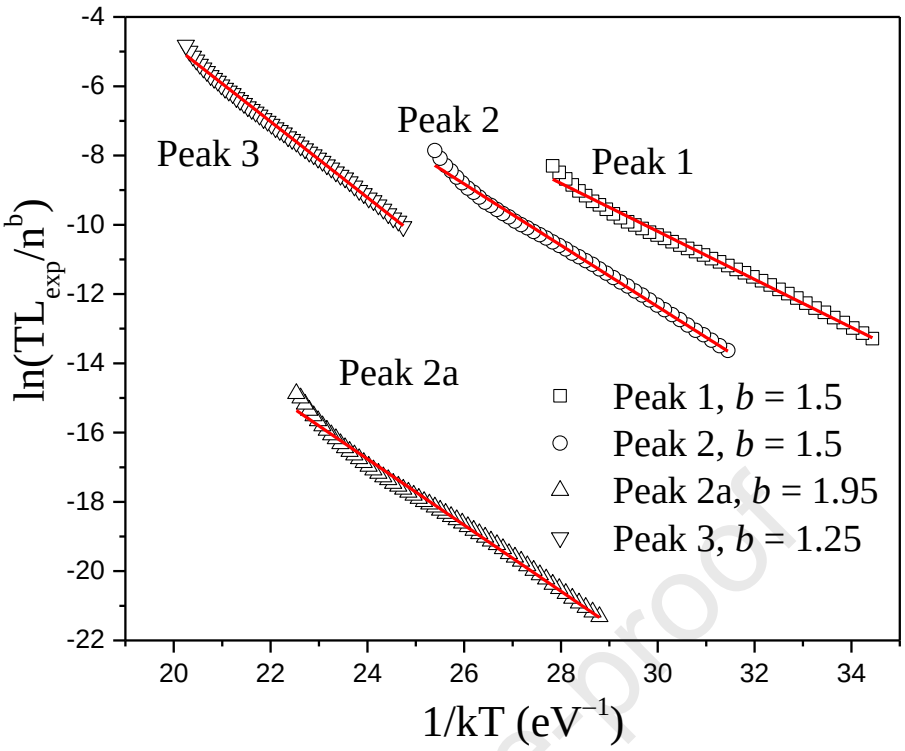

Figure 10. The plot of $\ln(TL_{exp}/n^b)$ against 1/kT for five peaks to the best fit of order of kinetics.

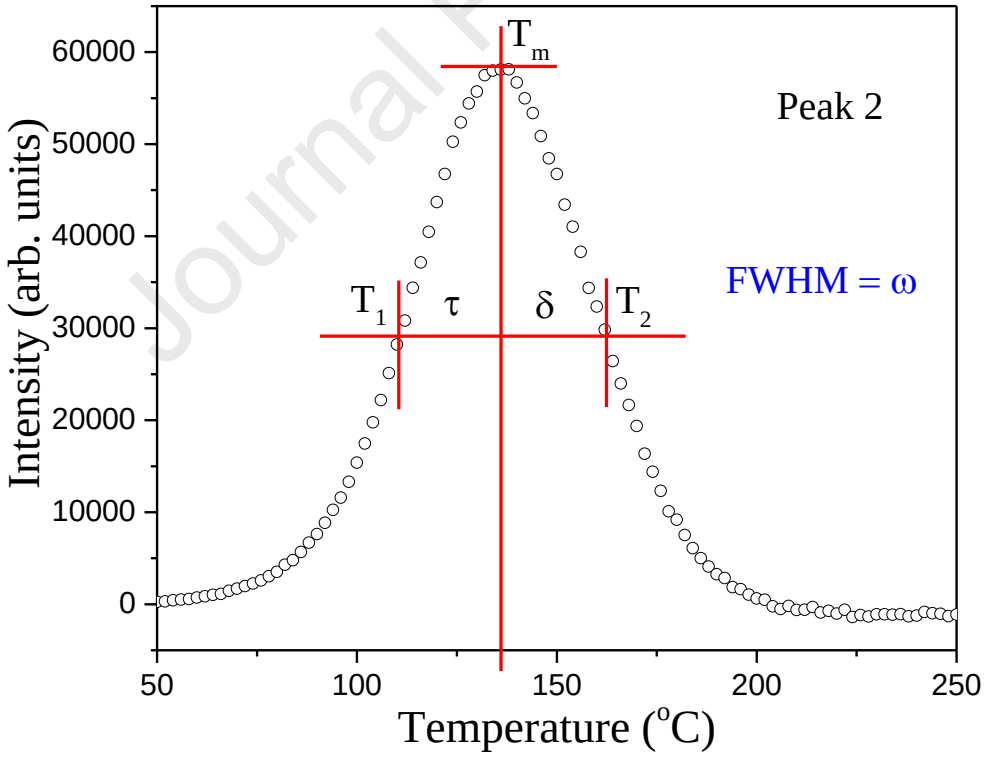

Figure 11. Kinetic analysis isolated peak 2 used in Chen peak shape method.

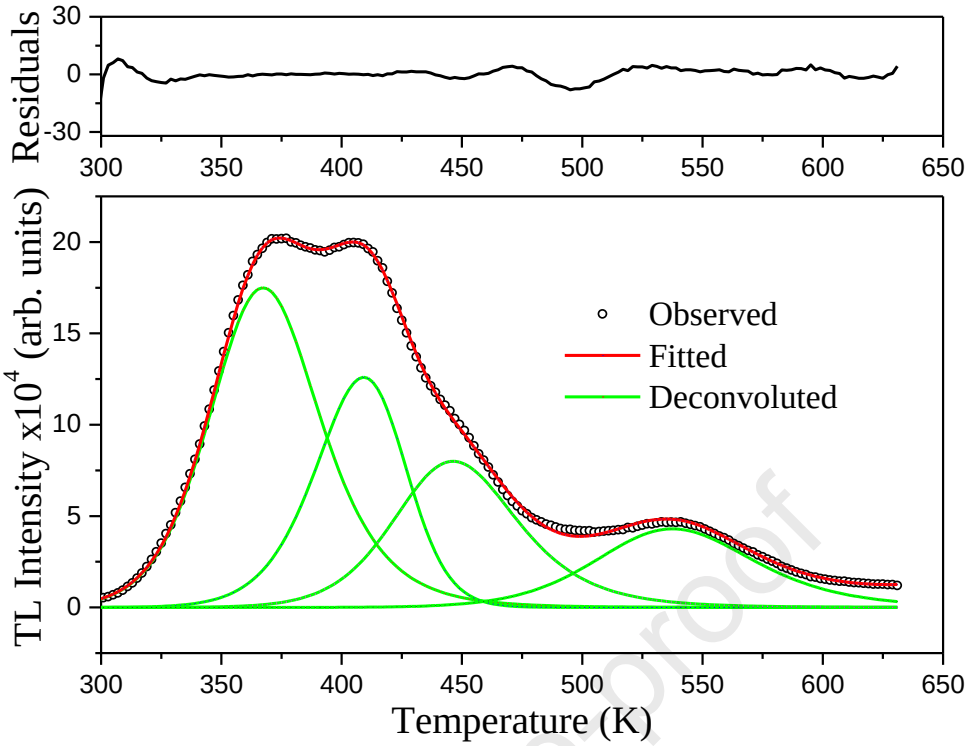

Figure 12. TL glow curve deconvolution of $SrAl_2O_4$ irradiated to 40 Gy.

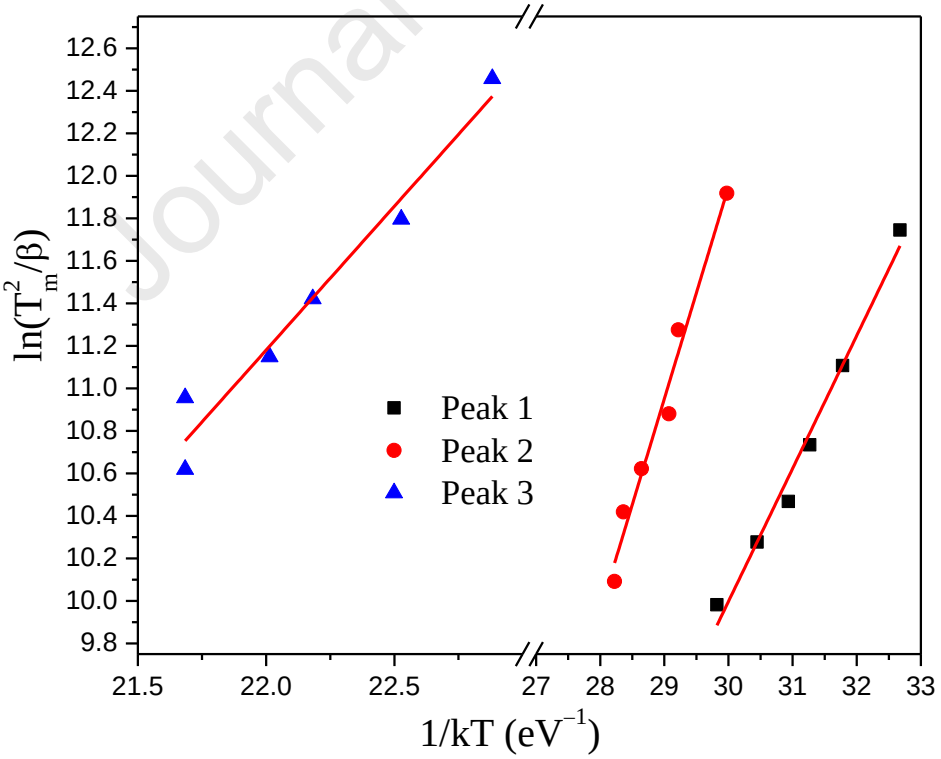

Figure 13. Plots of $\ln(T_m^2/\beta)$ as a function of $1/kT_m$ of the main TL peaks.

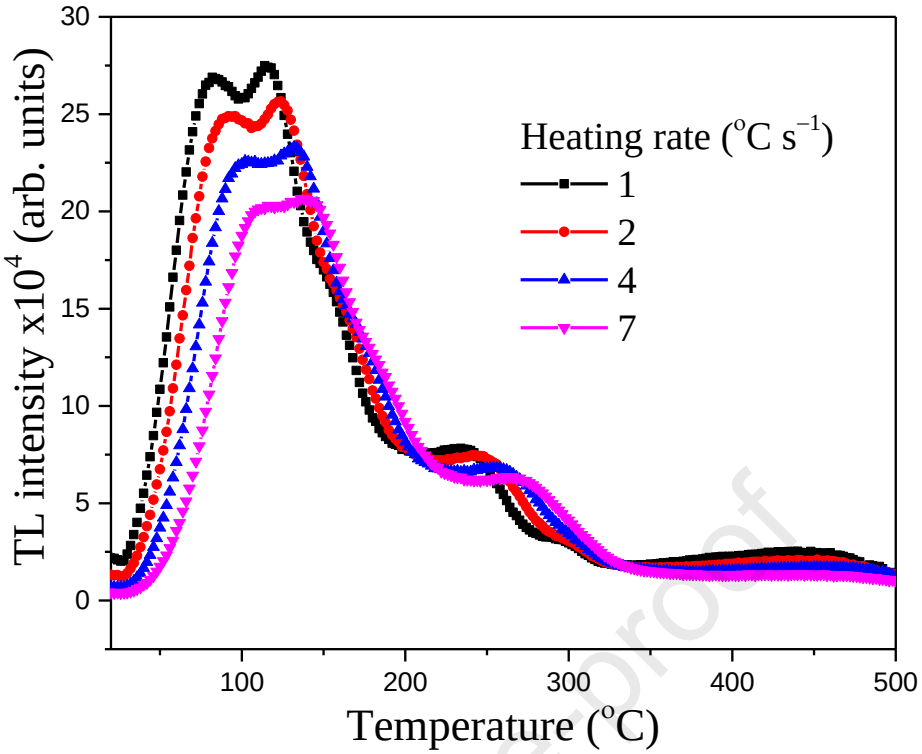

Figure 14. TL curves of $SrAl_2O_4$ irradiated to 40 Gy and measured at different heating rate.

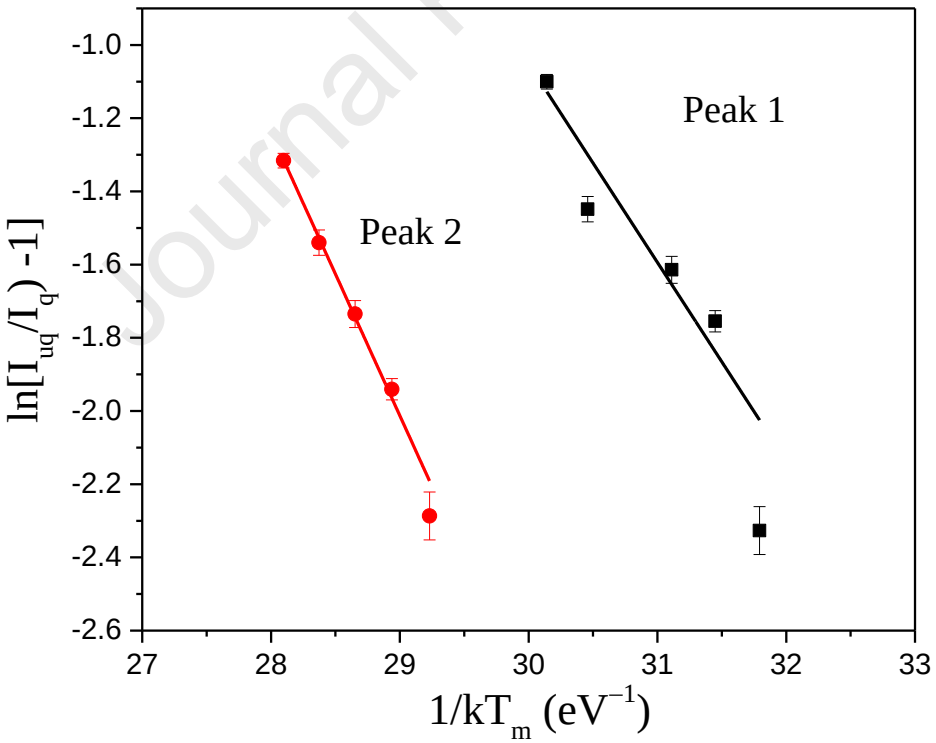

Figure 15. A plot of $\ln[(I_{uq}/I_q)-1]$ versus $1/kT_m$ for peak 1 and 2 intensity.

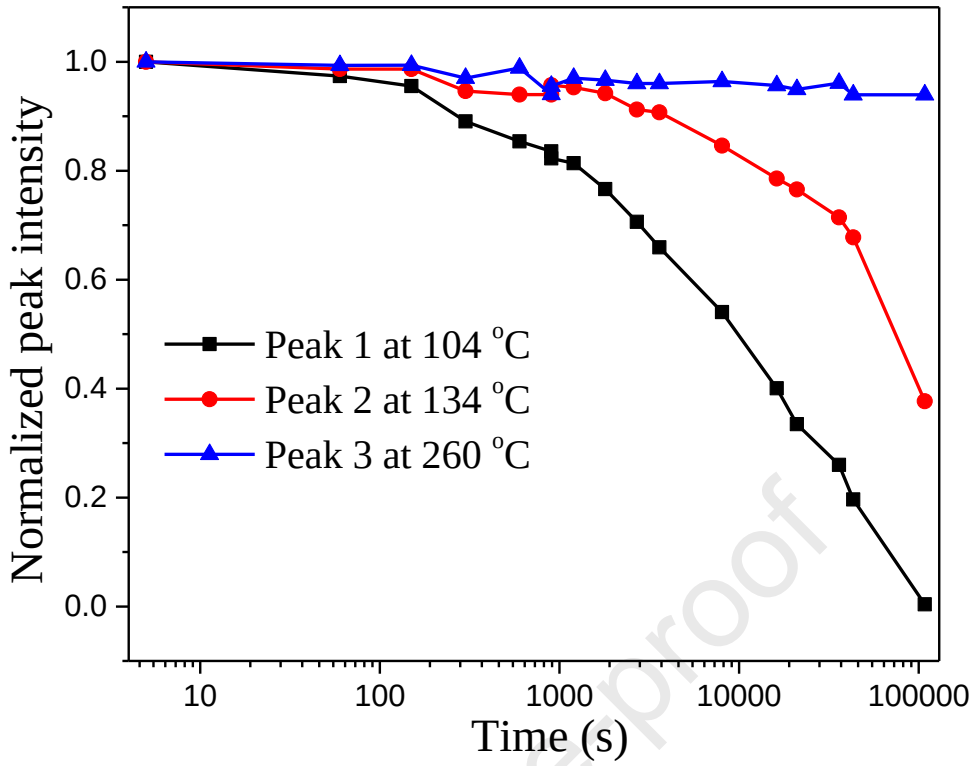

Figure 16. The change of TL peaks intensity with delay between irradiation and measurements.

Declaration of interests

☒ The authors declare that they have no known competing financial interests or personal relationships that could have appeared to influence the work reported in this paper.

☐ The authors declare the following financial interests/personal relationships which may be considered as potential competing interests: